Version of Record: https://www.sciencedirect.com/science/article/pii/S0022311521003202
Manuscript_f6b32223c36615a650fd83bafcfe0857

Improvement of the BISON U_3Si_2 modeling capabilities based on multiscale developments to modeling fission gas behavior

K. A. Gamble[a,*], G. Pastore[b], M. W. D. Cooper[c], D. A. Andersson[c], C. Matthews[c], B. Beeler[d], L. K. Aagesen[a], T. Barani[e], D. Pizzocri[e]

[a]*Computational Mechanics and Materials, Idaho National Laboratory, P.O. Box 1625, Idaho Falls, ID 83415-3840, USA*
[b]*Nuclear Engineering Department, University of Tennessee, Knoxville, TN 37996, USA*
[c]*MST-8, Materials Science in Radiation and Dynamics Extremes, Los Alamos National Laboratory, P.O. Box 1663, Los Alamos, NM 87545, USA*
[d]*Nuclear Engineering Department, North Carolina State University, Raleigh, NC 27695-7909, USA*
[e]*Politecnico di Milano, Department of Energy, Nuclear Engineering Division, Via La Masa 34, 20156 Milano, Italy*

Abstract

Uranium silicide (U_3Si_2) is a concept explored as a potential alternative to UO_2 fuel used in light water reactors (LWRs) since it may improve accident tolerance and economics due to its higher thermal conductivity and increased uranium density. U_3Si_2 has been previously used in research reactors in the form of dispersion fuel which operates at lower temperatures than commercial LWRs. The research reactor data illustrated that significant gaseous swelling occurs as the fuel burnup increases. Therefore, it is imperative to understand the fission gas behavior of U_3Si_2 under higher temperature LWR operating conditions. In this work, molecular dynamics and phase-field modeling techniques are used to reduce the uncertainty in select modeling assumptions made in developing the fission gas behavior model for U_3Si_2 in the BISON fuel performance code. To support the implementation of a U_3Si_2 fission gas model in BISON, cluster dynamics simulations of irradiation enhanced Xe diffusion have been carried out. Similarly, MD simulations were used to predict the athermal contribution due to atomic mixing during ballistic damage cascades. By combining our results with literature DFT data for thermal equilibrium diffusion, Xe diffusivity has been described over a wide range of temperatures for in-reactor conditions. These lower length scale informed models are then utilized in the assessment of BISON U_3Si_2 modeling capabilities by simulating the ATF-1 experiments irradiated in the Advanced Test Reactor (ATR). Sensitivity analysis (SA) and uncertainty quantification (UQ) are included as part of the assessment process to identify where further experiments and lower length scale modeling would be beneficial. The multiscale modeling approach utilized in this work can be applied to new fuel concepts being explored for both LWRs and advanced reactors (e.g., uranium nitride, uranium carbide).

Keywords: BISON, U_3Si_2, fission gas behavior, assessment, multiscale modeling

1. Introduction

Uranium silicide (U_3Si_2) is considered a potential replacement for UO_2 by both the U. S. Department of Energy's Advanced Fuels Campaign (AFC) and Westinghouse [1, 2] for improved accident tolerance in light water reactors (LWRs) due to its higher thermal conductivity, although Westinghouse's interest has dwindled recently. The higher thermal conductivity results in lower fuel centerline temperatures and shallower temperature gradients across the radius of the fuel. The lower temperature gradients decrease the likelihood of pellet cracking and subsequent radial relocation of the fuel fragments. Another advantage of U_3Si_2 is in terms of economics due to its higher uranium density, since it may enable higher burnups and longer cycle lengths.

One of the earliest publications on the irradiated behavior of U_3Si_2 (Shimizu [3]) was at power reactor temperatures. Until the recent post-irradiation examinations of U_3Si_2 by Cappia and Harp [4], Shimizu's work was the only U_3Si_2 data at LWR operating temperatures available in the literature. Since then, U_3Si_2 has been used in dispersion fuel in research reactors, so the majority of available experimental data is at these lower temperatures. Finlay et al. [5] observed that significant gaseous swelling occurs above a certain burnup associated with the so called "knee" phenomenon. Given the low temperatures of research reactors, the significant swelling was attributed to U_3Si_2 being amorphous under irradiation at these temperatures. Birtcher et al. [6] demonstrated that, under high-energy ion irradiation above 250°C, U_3Si_2 remains crystalline. This observation was confirmed by Miao et al. [7–9]. LWRs operate well above this threshold, so U_3Si_2 is expected to remain crystalline under irradiation in these reactors. Unfortunately, the gaseous fission product behavior and its impact on fuel performance is still not well understood for crystalline U_3Si_2 due to the lack of neutron irradiated data at LWR temperatures. Another concern with U_3Si_2 as a power reactor fuel is its relatively low melting

*Corresponding author
Email addresses: Kyle.Gamble@inl.gov (K. A. Gamble), gpastore@utk.edu (G. Pastore), cooper_m@lanl.gov (M. W. D. Cooper), andersson@lanl.gov (D. A. Andersson), cmatthews@lanl.gov (C. Matthews), bwbeeler@ncsu.edu (B. Beeler), Larry.Aagesen@inl.gov (L. K. Aagesen), tommaso.barani@cea.fr (T. Barani), davide.pizzocri@polimi.it (D. Pizzocri)

temperature (~1938 K).

The uncertainty associated with fission gas behavior under LWR operating conditions necessitates a mechanistic multiscale modeling approach. To enable fission gas behavior in U_3Si_2 to be accurately modeled in the BISON code, the Xe diffusivity must be defined. In UO_2, it is well known that there are three contributions to self- and Xe diffusivity for in-reactor conditions: i) thermal equilibrium diffusion (D_1), ii) irradiation enhanced diffusion (D_2), and iii) athermal diffusion due to atomic mixing during ballistic cascades (D_3). Unlike for UO_2, there is no experimental data for fission gas diffusivity in U_3Si_2. Therefore, atomic scale simulations can play a role in fulfilling this data need. Previously, DFT [10], cluster dynamics [11], and molecular dynamics (MD) [12] have been used to predict D_1, D_2, and D_3, respectively, for Xe diffusivity in UO_2. Having available experimental data to compare with enabled validation of these models and provides confidence that such approaches can also be applied to U_3Si_2 where validation data is lacking. Previously Andersson et al. [10] used DFT to predict the thermal equilibrium diffusivity of Xe, U and, Si in U_3Si_2. In doing so, they generated the necessary data to run cluster dynamics simulations of irradiation enhanced D_2 diffusion. Cooper et al. [13] used the data from Andersson et al. [10], to predict irradiation enhanced self-diffusion in U_3Si_2. Here, we extend that model to include Xe-containing defects to predict irradiation enhanced Xe diffusivity. Similarly to Cooper et al. [13], we have employed MD simulations of Xe in U_3Si_2 to predict the D3 term due to atomic mixing during ballistic cascades. The combined expressions for D_1, D_2, and D_3 can be used in the physics-based fission gas model in BISON.

In this paper, the models available in the BISON fuel performance code [14] for U_3Si_2 fuel along with their ranges of applicability and uncertainty are summarized. New updates to the parameters of the initial fission gas behavior model developed by [15], based upon molecular dynamics and phase-field analyses, is also presented. The paper concludes by revisiting a previous assessment [16] of the BISON U_3Si_2 modeling capabilities to the recent ATF-1 experiments irradiated in the Advanced Test Reactor (ATR), including sensitivity and uncertainty quantification analyses with the latest versions of the models and estimates of their uncertainty. Comparisons between the latest results and those from [16] to highlight the impacts of the improvements presented in this work are also included.

2. Thermo-mechanical Models for U_3Si_2

Multiple researchers have used BISON to analyze the fuel performance of U_3Si_2 during normal operating conditions [17, 18]. BISON contains a comprehensive set of thermo-mechanical properties for predicting the fuel performance of U_3Si_2 including thermal conductivity, specific heat, thermal expansion, elasticity, solid swelling, and creep. A coupled fission gas release and swelling model is also available and is described in Section 4.

A review of the already existing models in BISON for thermal conductivity, specific heat, thermal expansion, elasticity, and solid swelling models is provided. New developments in regards to lower length scale improvements in creep and fission gas behavior are also included.

2.1. Thermal properties

BISON contains many options for the thermal conductivity and specific heat capacity of U_3Si_2. The recommended correlations are those from the U_3Si_2 handbook [19]. The thermal conductivity correlation is a polynomial fit to the data of [3, 20–22]:

$$k = 9.029\times10^{-15}T^5 - 4.609\times10^{-11}T^4 + 8.676\times10^{-8}T^3 - 7.485\times10^{-5}T^2 + 4.166\times10^{-2}T + 0.5211 \quad (1)$$

where T is temperature in K. The correlation for the specific heat capacity is given as:

$$C_p = 1000.0\left(3.52\times10^{-5}T + 0.18\right) \quad (2)$$

where T is temperature in K and C_p is the specific heat capacity is in J/kg-K. The uncertainty in the thermal conductivity model is highlighted by Figure 1, which reproduces a plot similar to the one in the U_3Si_2 handbook [19], with dashed lines to represent the uncertainty assumed in the BISON model. The uncertainty is computed from the experimental data point with the largest deviation from the polynomial fit corresponding to the arc-cast data point at a temperature of ~1110 K with a thermal conductivity value of ~22.5 W/m-K. This calculation results in a 95% confidence band of ±18.2%. It should be noted that the induction cast data of [3] is not included in the uncertainty calculation, due to the measurements significantly underpredicting the thermal conductivity of U_3Si_2. The uncertainty in the specific heat capacity model is taken as ±3%, as per [23].

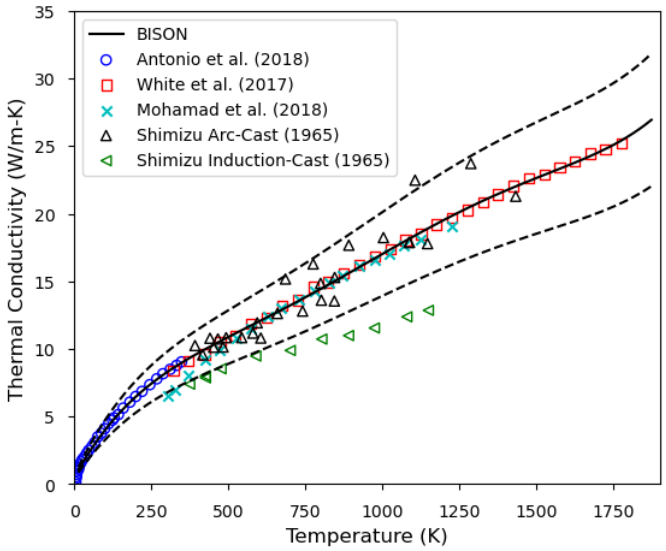

Figure 1: Handbook model with associated uncertainty represented by the dashed lines. Adapted from [19].

2.2. Elasticity

For mechanical analyses, U_3Si_2 is treated as an isotropic material. The elastic constants are determined using empirical fits to the data in the U_3Si_2 handbook [19]. The linear fits are illustrated along with the experimental data for the Young's modulus (black) and the shear modulus (blue) in Figure 2. To avoid cluttering the figure, equations of the linear fits are provided below.

The equation for Young's modulus is given by:

$$E = -6.695p + 137.55 \tag{3}$$

where E is the Young's modulus (GPa) and p is the porosity (%). The shear modulus is also a porosity-dependent function given by:

$$G = -2.833p + 56.938 \tag{4}$$

where G is the shear modulus (GPa). These equations are valid for porosity ranging from 1.5% to 10%. The theoretical density is taken as 12,200 kg/m^3, whereas the current density is calculated from the current fuel volume that accounts for thermal expansion, creep, solid swelling, densification, and gaseous swelling explained in subsequent subsections.

Given the limited amount of data for the elastic properties of U_3Si_2, the suggested model is designed to capture all of the data points in Figure 2 with a 95% confidence, assuming a normal distribution. Thus, the calculated uncertainty corresponds to two standard deviations about the mean determined by the correlations in Equations 3 and 4. The data points for the Young's (~151 GPa) and shear (~63 GPa) moduli from Mohamad et al. [21] are used to determine the bounds of the model given that it represents the furthest known value from the best-fit correlations. The calculated uncertainty is 29.1% and 26.8% for the Young's modulus and the shear modulus, respectively. The uncertainty ranges are included in 2 as dashed lines about the mean.

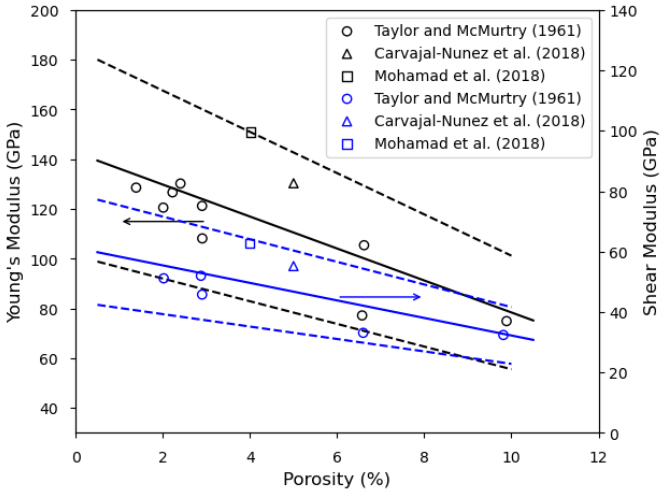

Figure 2: Young's and shear modulus data with trendline. Adapted from [19].

2.3. Thermal expansion

The U_3Si_2 handbook provides a temperature-dependent correlation for the instantaneous coefficient of thermal expansion (CTE). However, when including all of the data available for the CTE of U_3Si_2 (see Figure 3) it can be observed that assuming a constant value for all temperatures of $(16.0\pm3.0)\times10^{-6}$ K^{-1} captures all of the known experimental data. Since the available experimental data on thermal expansion of U_3Si_2 is limited this is the recommended value to use. Neutron diffraction measurements by [24] has shown that there is some anisotropy associated with the thermal expansion of U_3Si_2 at temperatures greater than 1000°C. In almost all cases analyzed in this work (see Section 5) the predicted temperatures remain below this threshold and therefore the anisotropy was not included in this work.

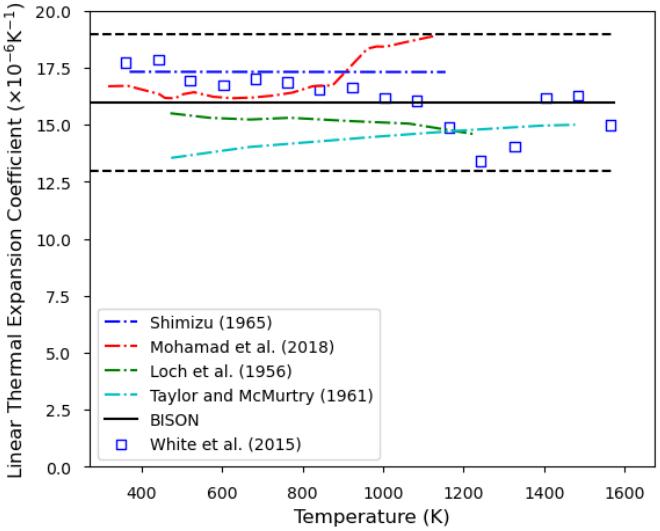

Figure 3: Linear thermal expansion coefficient data with the suggested constant value and uncertainty bands included. Based upon a figure from the U_3Si_2 handbook [19].

2.4. Creep

Prior to this work, the creep models for U_3Si_2 were empirical correlations (see [25, 26]) fit to the only experimental data available from the University of South Carolina [27]. Atomistic calculations were performed to develop a creep model containing contributions from three mechanisms of creep: Coble, Nabarro-Herring, and dislocation climb. The details on the derivation of the creep model can be found in [13]. Here, the final equations (as implemented into BISON) are shown.

The total creep rate is given by:

$$\dot{\epsilon} = \dot{\epsilon}_{NH} + \dot{\epsilon}_{Coble} + \dot{\epsilon}_{Climb} \tag{5}$$

where $\dot{\epsilon}_{NH}$, $\dot{\epsilon}_{Coble}$, and $\dot{\epsilon}_{Climb}$ are the contributions from Nabarro-Herring, Coble, and dislocation climb mechanisms, respectively

(s^{-1}). The Nabarro-Herring creep rate is given by:

$$\dot{\epsilon}_{NH} = \frac{\sigma}{d^2 T}\left[1.457\times10^{-11}\exp\left(\frac{-3.400}{k_B T}\right) + 5.081\times10^{-51}\dot{F}\exp\left(\frac{-0.540}{k_B T}\right)\right] \quad (6)$$

where σ is the effective stress (Pa), T is the temperature (K), d is the grain size (m), k_B is the Boltzmann constant (eV) and $\dot{F}$ is the fission rate density (fissions/m^3-s). Similarly, the Coble creep rate is given by:

$$\dot{\epsilon}_{Coble} = \frac{\sigma}{d^3 T}7.294\times10^{-20}\exp\left(\frac{-1.619}{k_B T}\right) \quad (7)$$

For dislocation climb the creep rate is:

$$\dot{\epsilon}_{Climb} = \frac{\sigma^3}{T}\left[1.512\times10^{-11}\exp\left(\frac{-4.160}{k_B T}\right) + 4.696\times10^{-55}\dot{F}\exp\left(\frac{-0.020}{k_B T}\right)\right] \quad (8)$$

The uncertainty in the lower length scale informed creep model is unknown. The model is included in the assessment studies completed in this work, but is not treated as an uncertain input.

2.5. Solid swelling

The total volumetric change due to swelling of the fuel is comprised of three components: solid and gaseous swelling, and densification. The behavior of solid fission products at LWR operating temperatures is expected to be similar to that at research reactor temperatures. Therefore, the solid swelling model in BISON is based upon the data from Hofman [28]. Hofman's data shows solid swelling as a function of the fission density in units of fissions/cm^3. To convert from fission density to units of burnup in fissions per initial metal atom (FIMA) (the units used in BISON), the fission density values are multiplied by a conversion factor of 3.635×10^{-23} cm^3/fission. After conversion, the correlation used is given by:

$$\left(\frac{\Delta V}{V}\right)_{solid} = 0.34392\,Bu \quad (9)$$

where $(\Delta V/V)_{solid}$ is the volumetric strain due to solid fission products and Bu is the burnup in FIMA. The uncertainty in solid swelling is assumed to be the same as for UO_2, given the fact that the correlation is also a linear function of burnup. This uncertainty is assumed to be ±20% [29].

2.6. Densification

The densification behavior of U_3Si_2 is unknown. It is believed that applying an empirical model for UO_2 as done in previous studies [16, 17] is unjustified, and therefore densification has been ignored in this work. Recent lower length scale work on microstructure effects on densification behavior in UO_2 [30] could be extended to fill the data gap on U_3Si_2 densification behavior in the future including low melting point secondary phases.

3. Development of the fission gas diffusivity model

Diffusion in nuclear fuel can exhibit three regimes: i) intrinsic diffusion at high temperatures (D_1), ii) irradiation-enhanced diffusion at intermediate temperatures (D_2), and iii) athermal diffusion at low temperatures (D_3). D_1 is thermally activated diffusion where defects are at thermal equilibrium concentrations. D_2 is due to thermal hopping of defects that have irradiation enhanced concentrations. D_3 is caused by atomic mixing during irradiation damage events. Due to a lack of experimental data for U_3Si_2, lower length scale (LLS) simulations have been used, in this work, to study diffusivity of fission gas under irradiation conditions. Andersson et al. [10] used DFT to calculate the diffusion coefficients for a range of Xe-containing defects in U_3Si_2. That work focused on diffusion under thermal equilibrium (D_1) but, in doing so, generated all of the necessary data for cluster dynamics simulations of irradiation enhanced diffusion.

3.1. Centipede

To study irradiation-enhanced diffusivity in U_3Si_2, cluster dynamics simulations have been used to predict the steady state concentration of defects. In previous work [13], we used the Centipede code to simulate irradiation-enhanced self-diffusion of U and Si based on Frenkel production due to irradiation, annihilation at sinks, and mutual recombination. Here we build upon that model by including Xe-containing defect clusters. Although the Centipede code has been discussed in detail elsewhere [11, 31], here we give a brief overview of the methodology for completeness.

The concentrations of defects in the system are calculated by solving a set of ordinary differential equations (ODEs) that capture a number of phenomena including: production of Frenkel pairs through irradiation, mutual recombination of Frenkel pairs, interaction with sinks, and clustering of point defects. For a given defect concentration, x_d, the ODE can be expressed as:

$$\frac{\mathrm{d}x_d}{\mathrm{d}t} = \dot{\beta}_d + \sum_C \dot{R}_{d,C}(x_d, x_C, T, G) - \sum_s \dot{S}_{d,s}(x_d, x_s, T, G) \quad (10)$$

where $\dot{\beta}_d$ describes the source rate of defects through radiation damage. $\dot{R}_{d,C}$ and $\dot{S}_{d,s}$ are the cluster and sink rates, which are summed across individual cluster and sink types, respectively. The Centipede code finds the steady-state solution to this coupled set of ODEs, such that $\frac{dx_d}{dt} \leq \mathcal{R}$ for all defects, where $\mathcal{R}$ is a convergence criteria. An individual reaction rate, $\dot{R}_d$, can be expressed as:

$$\dot{R}_d = \begin{cases} \frac{k_i^2}{\Omega} D x_A x_B \left[1 - exp\left(\frac{f}{k_B T}\right)\right], & \text{if } f < 0, \\ \frac{k_i^2}{\Omega} D x_Y x_Z \left[exp\left(\frac{f}{k_B T}\right) - 1\right], & \text{otherwise} \end{cases} \quad (11)$$

where Ω is the atomic volume, k_i is a reaction rate constant, $D = D_A + D_B$ is the sum of the diffusivities of the reactants (labeled A and B), x_A and x_B are the concentrations of the reactants and x_Y and x_Z are the concentrations of the products (labeled Y and Z). If $f < 0$ the net rate is for the reaction to go forwards and otherwise it goes backwards. The driving force is given by the change in the free energy of the system due to the reaction:

$$f = \sum_{p \epsilon P} \frac{\partial G}{\partial x_p} - \sum_{r \epsilon R} \frac{\partial G}{\partial x_r} \tag{12}$$

where P and R are the set of products, p, and reactants, r, respectively. A detailed explanation of Eqs. (10) to (12) and their application to UO_2 is given in by Matthews et al. [11, 31].

3.2. Cluster dynamics simulations for D_1 and D_2

The total concentration of Xe in the lattice is governed by the processes of fission (sourcing), and trapping and resolution at intra-granular bubbles. These processes are not considered within the Centipede code but are instead taken into account by the fission gas release model within BISON. The concentration of Xe in the lattice is, thus, treated as fixed during the cluster dynamics simulations. The Xe diffusivity is defined by a sum over all Xe-containing defects, i:

$$D_{Xe} = \frac{\sum_x c_x D_x}{\sum_x c_x} \tag{13}$$

where D_x and c_x are the diffusivity and concentration of defect x. Given that the total Xe diffusivity is independent of the Xe concentration, the absolute formation energies of the Xe-containing defects do not influence the diffusion coefficient. Instead, only the relative energies are considered. The reference Xe-containing defect has been taken to be a Xe interstitial, Xe_i. All other Xe-containing defects (e.g. Xe_U and Xe_{Si}) have been treated as clusters, whereby the binding energy with respect to the constituent point defects is used within the Centipede code. The following reaction defines the binding energy:

$$Xe_i + nV_U + mV_{Si} \rightarrow \{Xe : nV_U : mV_{Si}\} \tag{14}$$

where n and m are the number of V_U and V_{Si} point defects that make up the cluster, and standard Kröger-Vink notation has been used, except with charges omitted due to the metallic-bonding of U_3Si_2. Clusters consisting of more than one vacancy are denoted using braces. For example, $\{Xe : V_U : V_{Si}\}$ represents a cluster containing one U vacancy, one Si vacancy, and a Xe atom but without specifying the exact site that Xe occupies within the vacancy cluster.

The binding energies, H_B, and entropies, S_B, for all defect clusters considered are determined from the data in Andersson et al. [10] and are summarized in Table 1, alongside the point defect formation energies, H_f, and entropies, S_f. Negative and positive values for the binding energy and entropy, respectively, contribute to favorable binding.

The parameters in Table 1 govern the stability of defects under thermal equilibrium. However, the diffusivity of the defects is also critical to modeling the irradiation enhanced concentrations of defects. The diffusivity of a defect, x, is given by:

$$D_x = \frac{Z}{2\xi} \alpha^2 \upsilon_{mig} \exp\left(\frac{-H_{mig}}{k_B T}\right) \tag{15}$$

where H_{mig} is the defect migration barrier, υ_{mig} is the attempt frequency, Z is the number of jump directions, α is the jump distance, and ξ is the dimensionality of diffusion. Diffusion in U_3Si_2 is highly anisotropic due to the tetragonal crystal structure. However, if two point defects come into contact, the subsequent reaction is agnostic of the crystallographic direction that the defect arrived from. Therefore, the defect reactions that are being solved for will be dominated only by diffusion in the fastest direction. The parameters for diffusion in the fastest direction for each defect, as used in Centipede, are taken from Andersson et al. [10] and are summarized in Table 2.

The parameters for defect stability and diffusion were implemented in the Centipede code to determine the irradiation enhanced defect concentrations for Xe-containing clusters in U_3Si_2. When solving for the steady-state concentrations, the following defect reactions were included:

Table 1: Point defect formation energies and entropies, and the cluster binding energies and entropies, from Andersson et al. [10], used in the cluster dynamics model.

Point Defect	H_f (eV)	S_f (k_B)	n
U_i	0.87	-3.15	2
V_U	1.69	0.45	1
Si_i	0.55	2.19	1
V_{Si}	1.79	6.28	2
Cluster	**H_B (eV)**	**S_B (k_B)**	**n**
Xe_U	-2.12	-1.88	1
Xe_{Si}	-2.10	-9.32	1
$\{Xe : 2V_U\}$	-2.61	-2.59	1
$\{Xe : 2V_{Si}\}$	-2.05	-9.32	1
$\{Xe : V_U : V_{Si}\}$	-3.35	-4.19	1

Table 2: Parameters that describe the point defect and cluster diffusivities, from Andersson et al. [10], used in the cluster dynamics model. The impurity defect Xe_U and Xe_{Si} are immobile and are, as such, omitted.

Point Defect	H_{mig} (eV)	υ_{mig} (Hz)	α (Å)	ξ	Z
U_i	0.31	1.51×10^{14}	3.80	2	4
V_U	1.21	1.40×10^{13}	3.90	1	2
Si_i	1.80	1.00×10^{13}	5.18	2	4
V_{Si}	2.37	1.00×10^{13}	4.19	2	4
Xe_i	3.13	1.00×10^{14}	3.90	1	2
Cluster	**H_{mig} (eV)**	**υ_{mig} (Hz)**	**α (Å)**	**ξ**	**Z**
$\{Xe : 2V_U\}$	1.68	1.00×10^{13}	3.90	1	2
$\{Xe : 2V_{Si}\}$	2.33	1.00×10^{13}	4.19	2	4
$\{Xe : V_U : V_{Si}\}$	2.61	1.00×10^{13}	4.19	2	4

Reactions of U and Si defect with sinks

$$sink + U_i \leftrightarrow sink + V_i \quad (16)$$
$$sink + Si_i \leftrightarrow sink + V_i \quad (17)$$
$$sink + V_U \leftrightarrow sink + U_U \quad (18)$$
$$sink + V_{Si} \leftrightarrow sink + Si_{Si} \quad (19)$$

Binding reactions

$$Xe_i + V_U \leftrightarrow Xe_U + V_i \quad (20)$$
$$Xe_i + V_{Si} \leftrightarrow Xe_{Si} + V_i \quad (21)$$
$$Xe_U + V_U \leftrightarrow \{Xe : 2V_U\} \quad (22)$$
$$Xe_{Si} + V_{Si} \leftrightarrow \{Xe : 2V_{Si}\} \quad (23)$$
$$Xe_U + V_{Si} \leftrightarrow \{Xe : V_U : V_{Si}\} \quad (24)$$
$$Xe_{Si} + V_U \leftrightarrow \{Xe : V_U : V_{Si}\} \quad (25)$$

Recombination of interstitials and vacancies

$$U_i + V_U \leftrightarrow U_U + V_i \quad (26)$$
$$Si_i + V_{Si} \leftrightarrow Si_{Si} + V_i \quad (27)$$
$$U_i + \{Xe : 2V_U\} \leftrightarrow Xe_U + U_U + V_i \quad (28)$$
$$Si_i + \{Xe : 2V_{Si}\} \leftrightarrow Xe_{Si} + Si_{Si} + V_i \quad (29)$$
$$U_i + \{Xe : V_U : V_{Si}\} \leftrightarrow Xe_{Si} + U_U + V_i \quad (30)$$
$$Si_i + \{Xe : V_U : V_{Si}\} \leftrightarrow Xe_U + Si_{Si} + V_i \quad (31)$$

Kickout reactions

$$U_i + Xe_U \leftrightarrow U_U + Xe_i \quad (32)$$
$$Si_i + Xe_{Si} \leftrightarrow Si_{Si} + Xe_i \quad (33)$$

The system was evolved using the Centipede code until it reached steady-state, whereby the rate of change of all defect concentrations, due to the above reactions, tends to zero. When determining the diffusivity of Xe, the relative concentration of each defect is the parameter of interest, rather than the absolute concentration, which is solved separately in BISON based on interactions of Xe with intra-granular bubbles. Figure 4 shows the concentrations of Xe-containing clusters relative to the total Xe concentration in U_3Si_2. For comparison, the relative concentrations at thermal equilibrium are also shown using dashed lines. It can be seen that there is very limited irradiation-enhancement of defect concentrations over a wide range of temperatures. In fact, for all defects other than a Si di-vacancy containing a Xe atom, $\{Xe : 2V_{Si}\}$, the irradiation enhancement is negligible over the full temperature range that has been studied (600 – 1500 K). As has been shown in previous work by Cooper et al. [13], of the host U and Si defects, only V_{Si} is significantly enhanced due to irradiation. As a pre-cursor to the formation of $\{Xe : 2V_{Si}\}$, this translates into an irradiation enhanced concentration of $\{Xe : 2V_{Si}\}$.

Figure 5 shows the contribution to total Xe diffusivity due

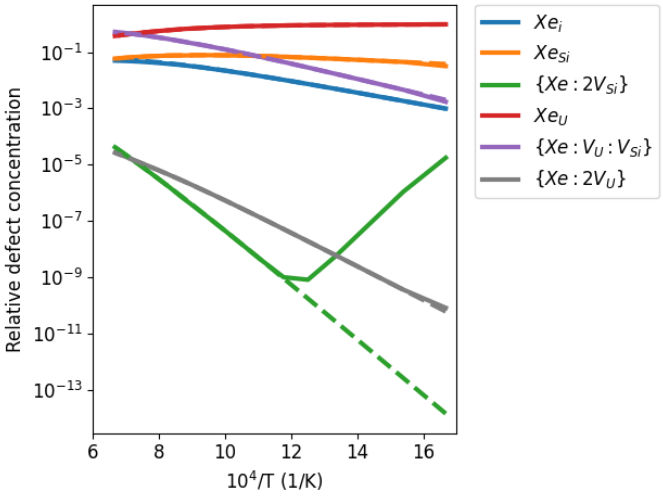

Figure 4: The relative concentrations of various Xe-containing defects in U_3Si_2 under irradiation predicted by cluster dynamics simulations. The irradiation-enhanced and thermal equilibrium results are shown by solid and dashed lines, respectively.

to various Xe-containing defects under irradiation, calculated using Eq. (13)). This is determined by multiplying the relative concentration of a given defect (shown in Fig. 4) by the diffusivity of that defect, as defined by the data in Table 2. Similar to the results shown in Fig. 4, there is no enhanced-diffusivity for any defects, except $\{Xe : 2V_{Si}\}$, which is enhanced below 850 K. However, $\{Xe : 2V_{Si}\}$ does not dominate diffusivity above 600 K and, therefore, irradiation-enhanced D_2 diffusion is not expected to dominate at temperatures experienced in LWRs.

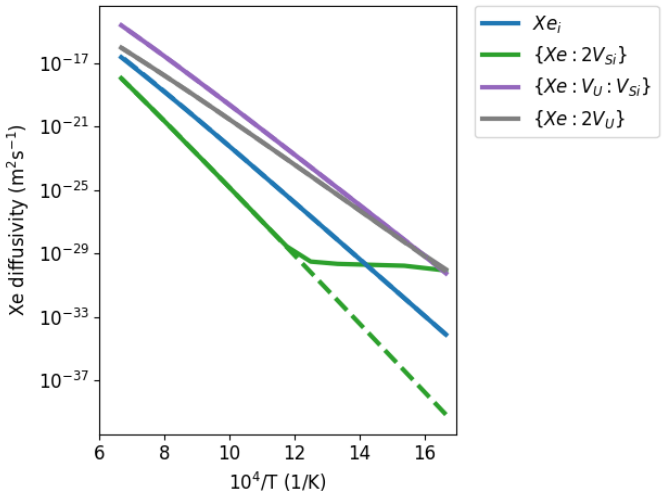

Figure 5: The dseciffusivity of various Xe-containing defects in U_3Si_2 under-irradiation predicted by cluster dynamics simulations. The irradiation-enhanced and thermal equilibrium results are shown by solid and dashed lines, respectively.

In future work, the cluster dynamics model developed here could be expanded to account for the evolution of sinks (e.g., dislocations and bubbles) and thermochemistry as a function of burnup. If DFT data were to be generated for the stability and

diffusivity of other fission products, a similar approach could be used to create diffusion coefficients to describe a broader range of mechanisms that impact fuel performance (e.g., solid-swelling).

3.3. MD simulations of D_3

While we do not expect a D_2 contribution to Xe diffusivity, we must still consider the possibility of the athermal D_3 contribution, which is caused by atomic mixing during damage events. D_3 may have contributions due to atomic mixing during both electronic and ballistic stopping. While significant atomic mixing during electronic mixing is expected in insulating materials such as UO_2, materials like U_3Si_2 that exhibit high electronic heat transfer are expected to rapidly dispensate the energy of a thermal spike before significant energy is deposited into the lattice. Therefore, we have only considered the contributions to D3 from atomic mixing during ballistic cascades. To investigate this, MD simulations were carried out using the Large-scale Atomic/Molecular Massively Parallel Simulator (LAMMPS) code [32] with the interatomic forces for U_3Si_2 and Xe in U_3Si_2 given by the MEAM potential of Beeler et al. [33, 34]. A 30×30×30 supercell of U_3Si_2, where 1% of the U atoms were replaced with Xe, was equilibrated at 600 K for 15 ps in the NPT ensemble, with the supercell dimensions averaged over the final 5 ps. By fixing the supercell geometry at the averaged values, MD simulations of ballistic cascades were carried out in the NVE ensemble using PKA energies of 1 keV, 2 keV, and 3 keV. As discussed previously, very small timesteps had to be used to ensure conservation of energy during the simulation. This made it too difficult to carry out simulations of PKA energies greater than 3 keV. A 0.001 fs timestep was used for the first 0.5 ps, followed by 0.003 fs for 3 ps, then 0.01 fs for 10 ps, and 0.1 fs for the remaining 16.5 ps. The simulations were repeated three times for each energy using a random orientation for the PKA velocity each time.

During the simulations the mean squared displacement (MSD) of the Xe atoms was computed. Figure 6 shows the MSD as function of time for Xe, U, and Si during a 3 keV cascade. The data for U and Si are from a similar study by Cooper et al. [13], whereas the Xe data was calculated here. For all species there is an initial rapid increase in the MSD, followed by some oscillations that eventually dissipate. For the 3 keV cascade shown in Fig. 6, the Xe atoms were displaced less significantly than the U and Si atoms.

For a given PKA energy, the final MSD is taken by averaging over the final 16 ps of each simulation and then averaging again over three such cascade simulations. The MSD is shown as a function of the PKA energy per unit supercell volume in Fig. 7. It can be seen that Xe is displaced to a lesser extent than either U or Si for all PKA energies considered; except in the 1 keV cascades, where it is displaced marginally more than Si. Therefore, the athermal diffusivity in U_3Si_2 due to ballistic mixing is expected to be lower for Xe than for U or Si. One possible explanation for the lower displacement of Xe could be that U and Si interstitial migration barriers are quite low compared to those for Xe, indicating that lower barriers must be overcome for the displacement of U and Si during the cascade.

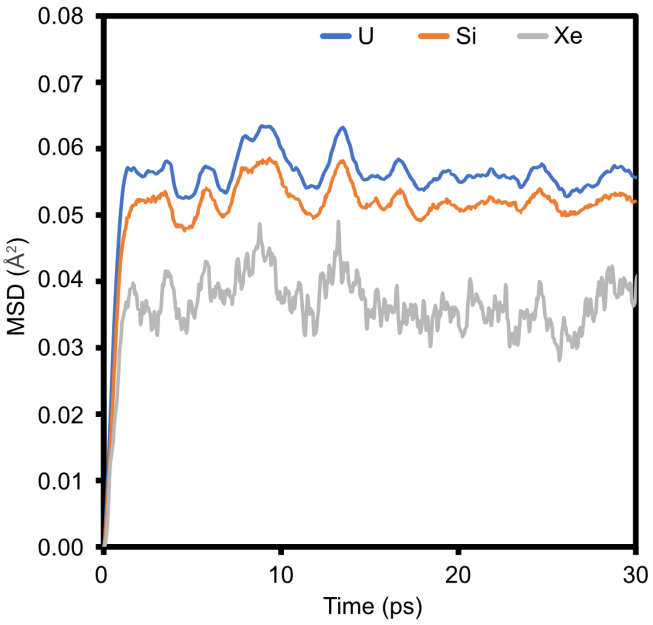

Figure 6: The MSD of Xe (gray) as a function of time during a ballistic cascade in U_3Si_2. The data from a similar cascade simulation carried out by Cooper et al. [13] for U (blue) and Si (orange) in U_3Si_2 are included for comparison.

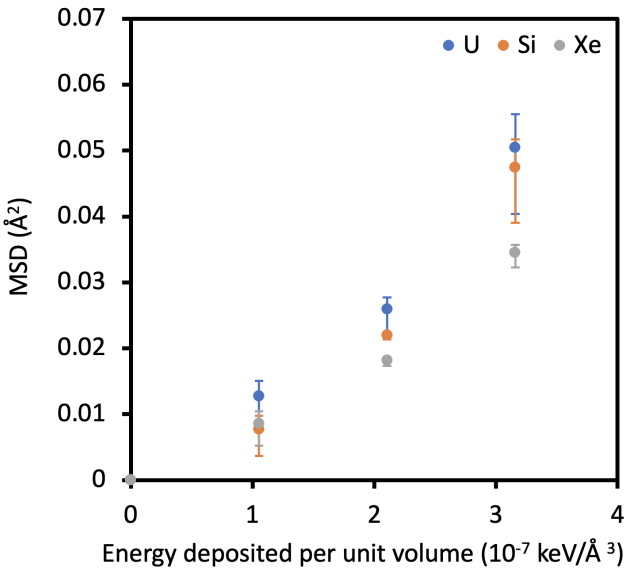

Figure 7: The MSD of Xe (gray) averaged over the final 15 ps of cascade simulations at 600 K as a function of PKA energy deposited per unit volume. The data from Cooper et al. [13] for U (blue) and Si (orange) are included for comparison. Each data point is the average of three cascade simulations and the range of these three values for each PKA energy is shown by the error bars.

The slope of the data in Fig. 7 defines the extent of atomic mixing for a given amount of energy deposited by a PKA. In nuclear fuel, high energy fission fragments deposit energy into the lattice through damage cascades (ballistic stopping) and thermal spikes (electronic stopping). Both of these processes could, in

Table 3: The ϵ_B, A_B, and D_3 parameters for Xe in U_3Si_2. E_F is taken to be 170 MeV and it is assumed 10 % of this energy is deposited through ballistic stopping. D_3 values assume a fission rate density of 10^{19} $m^{-3}s^{-1}$. These assumptions can be modified depending on reactor design or local irradiation conditions.

Species	ϵ_B (m^5MeV^{-1})	A_B (m^5)	D_3 (m^2s^{-1})
U [13]	1.46×10^{-42}	4.15×10^{-42}	4.15×10^{-23}
Si [13]	1.32×10^{-42}	3.73×10^{-42}	3.73×10^{-23}
Xe	1.01×10^{-42}	2.86×10^{-42}	2.86×10^{-23}

principle, contribute to the athermal diffusion coefficient:

$$D_3 = D_B + D_E \tag{34}$$

where D_B and D_E are the contributions to athermal diffusion from ballistic and electronic stopping, respectively. We assume that, unlike in UO_2 (an insulator), energy deposited electronically in U_3Si_2 (metal-like) is rapidly dissipated due to the high electronic thermal conductivity of the system [23]. Therefore, we consider energy deposited electronically as not contributing to atomic mixing. Instead, only the remaining 10% of energy that is deposited ballistically contributes to athermal diffusion, such that, following a similar approach to that carried previously on other fuels [12, 35]:

$$D_3 = A\dot{F} \tag{35}$$

$$A = \frac{0.1}{6}\epsilon_B E_F \tag{36}$$

where $\dot{F}$ is the fission rate per unit volume, and A is the constant of proportionality between D_3 and $\dot{F}$. ϵ_B is the MSD per unit energy deposited in a unit volume of lattice due to ballistic damage cascades, which is determined by the slope of a linear fit to the date in Fig. 7. The factor of 1/6 accounts for diffusion in three dimensions, given that the directions of PKAs due to ballistic stopping are randomized. The energy released due to a single fission event, E_F, is taken as 170 MeV. The factor of 0.1 accounts for the fact that, as discussed previously, only 10% of E_F is deposited ballisticaly in U_3Si_2 (based on the value for UC being representative of U_3Si_2, using the same assumption as in Matthew et al. [36]).

Table 3 shows the values of E_B, A, and D_3 for Xe in U_3Si_2 based on a typical $\dot{F}$ of 10^{19} $m^{-3}s^{-1}$ for LWR conditions. For comparison, the values for U and Si from Cooper et al. [13] are also shown. As already discussed in relation to Figs. 6 and 7, Table 3 shows D_3 is lower for Xe than it is for U or Si. More importantly, D_3 for Xe is higher by several orders of magnitude than irradiation-enhanced diffusion (D_2), as determined from cluster dynamics simulations (Section 3.2). Therefore, the diffusivity of Xe for in-reactor conditions can be described over a wide temperature range by D_1 and D_3 contributions only.

Stoichiometric conditions:

$$D_{Xe} = D_1 + D_3 \tag{37}$$

$$D_{Xe} = 4.82 \times 10^{-5} \exp\left(\frac{-3.04}{k_B T}\right) + 2.86 \times 10^{-42}\dot{F} \tag{38}$$

where D_{Xe} represents the Xe diffusion coefficient in m^2/s and $\dot{F}$ is the fission rate density in fissions/m^3-s, k_B is the Boltzmann constant in eV/K and T is the temperature in K.

This LLS-informed Xe diffusion coefficient has been used to inform a stoichiometric U_3Si_2 fission gas swelling and release model, as described in Section 4. Given the extremely high energy nature of ballistic cascades, we have assumed that D_3 is insensitive to changes in chemistry, whereas for D_1 a modification can be provided based on the results from Andersson et al. [10] to account for Si-rich conditions. U-rich conditions have been omitted given that Middleburgh et al. only predicted significant deviation from stoichiometric U_3Si_2 on the Si-rich side of the phase diagram [10, 37].

Si-rich conditions:

$$D_{Xe} = 7.22 \times 10^{-6} \exp\left(\frac{-2.84}{k_B T}\right) + 2.86 \times 10^{-42}\dot{F} \tag{39}$$

Figure 8 presents the total Xe diffusivity for both stoichiometric and Si-rich U_3Si_2 in comparison to the Turnbull model for UO_2 [38, 39]. It can be seen from Figure 8 that at low temperatures the athermal Xe diffusivity in U_3Si_2 is lower than that in UO_2. The thermal equilibrium contribution has a stronger temperature dependence in U_3Si_2 than in UO_2, resulting in higher diffusivity than in UO_2 at high temperatures. It is clear that the behavior of U_3Si_2 with respect to UO_2, will be highly sensitive to the fuel temperatures during reactor operating conditions and must be examined using fuel performance simulations. Additionally, the difference in Xe diffusivity in U_3Si_2 under Si-rich and stoichiometric conditions is not very significant and is within the uncertainty of the diffusion coefficients. This indicates that Xe diffusivity will not be particularly sensitive to thermodynamics conditions.

4. Gaseous swelling and fission gas release

The BISON model for fission gas evolution in U_3Si_2 incorporates the fundamental physical mechanisms of fission gas behavior and calculates the coupled fission gas release (FGR) and gaseous swelling concurrently. Given the lack of experimental data for U_3Si_2 under LWR conditions, a multiscale approach has been adopted for model development, with the engineering BISON model being informed by parameters calculated via atomistic and meso-scale simulations, as described in Section 3. Considering that U_3Si_2 under LWR conditions retains a polycrystalline structure, fission gas behavior is modeled as consisting of two main stages (intra-granular and inter-granular behavior) analogous with UO_2. The intra-granular component is based on a reduced-parameter cluster dynamics model and computes the evolution of intra-granular fission gas bubbles and

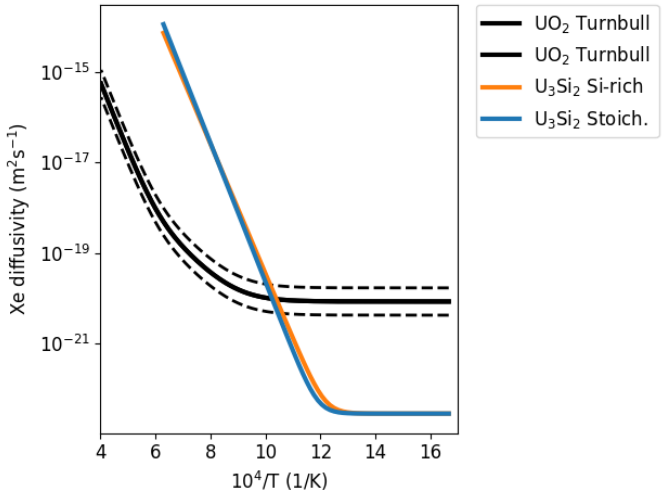

Figure 8: The total Xe diffusivity in stoichiometric and Si-rich U_3Si_2 given by equations 38 and 39 respectively. The Turnbull UO_2 model is shown for comparison [38, 39]. A factor of ×2 and ×0.5 have been applied the Turnbull model to approximate the range of data sown in Turnbull et al. [38].

swelling coupled with gas diffusion to grain boundaries. The inter-granular component describes the evolution of grain-boundary fission gas bubbles coupled to fission gas release, based on the approach developed for UO_2 in [40], modified by the usage of specific U_3Si_2 parameters. The current BISON model is based on the development described in [15]. However, improvements have been made in the present version, based on recent lower length scale calculations. In particular, these include the atomistic calculations to better assess the diffusion coefficients of fission gas atoms and vacancies in U_3Si_2, as described in Section 3. The latest model, applied in the present work, also includes improved parameters based on molecular dynamics calculations in [41] and the phase-field calculations of [42].

The molecular dynamics calculations by [41] determined an improved value for the surface energy of 1.7 ± 0.85 J/m^2. Also, based on [41], an improved estimate for the semi-dihedral angle of lenticular grain-boundary fission gas bubbles, θ, was developed to be $\theta = 73°$. The uncertainty on the semi-dihedral angle is assumed to be a uniform scaling factor between 0.5 and 1.0. This is to ensure that the uncertainty range does not extend towards the unrealistic theoretical value of 90° while still bounding the nominal value for UO_2 of 50° used in previous studies [16]. The phase-field calculations by [42] calculated a more realistic value of 0.6 ± 0.072 for the fractional coverage of grain boundaries at saturation, known as $F_{c,sat}$. The uncertainties in both the surface energy and saturation coverage are assumed to be 95% confidence (i.e., two standard deviations).

Atomic scale simulations have been used to investigate the irradiation-enhanced Xe diffusivity in Section 3, combined with the thermal equilibrium data from Andersson et al. [10]. Equations (38) and (39) for the unperturbed fission gas diffusivity can be implemented directly into the fission gas release model in BISON. Due to the inclusion of Xe athermal diffusion in Eqs. (38) and (39), the model can be applied over a wide range of temperatures and fission rates.

Another important component of the fission gas release model is the diffusion of vacancies to inter-granular bubbles that enable the bubbles to swell and reach their equilibrium pressure. Building upon the thermal equilibrium DFT study of Andersson et al. [10], Cooper et al. [13] examined the irradiation-enhanced diffusivity for U and Si defects in U_3Si_2 in the context of self-diffusion and creep. They found that for all temperatures the bulk diffusivity of V_{Si} was lower than that of V_U. Given that stoichiometry must be maintained for significant bubble growth to occur, this makes V_{Si} the rate limiting process for bubble swelling. Note that D_3 is excluded from vacancy diffusion since the disorder during a cascade means that tracking the displacement of individual vacancies loses its meaning. Instead the second term in Eqs. (40) and (41) is due to the irradiation enhanced D_2 regime. D_1 and D_2 have been determined by fitting to the cluster dynamics simulations from Cooper et al. [13] for V_{Si} in the bulk lattice.

Stoichiometric conditions:

$$D_v = 9.37 \times 10^{-4} \exp\left(\frac{-4.16}{k_B T}\right) + 1.97 \times 10^{-47} \dot{F} \qquad (40)$$

where D_v represents the bulk Si vacancy diffusivity in m^2/s and $\dot{F}$ is the fission rate density in fissions/m^3-s, k_B is the Boltzmann constant in eV/K and T is the temperature in K. Similar to Xe diffusion, the D_1 contribution is sensitive to changes in chemistry and, as such, based on the data from Andersson at al. [10], D_1 has been adjusted for Si-rich conditions.

Si-rich conditions:

$$D_v = 9.76 \times 10^{-5} \exp\left(\frac{-4.22}{k_B T}\right) + 1.97 \times 10^{-47} \dot{F} \qquad (41)$$

Equations 40 and 41 are then modified to estimate the grain boundary diffusivity, to describe the rate of vacancies arriving at inter-granular bubbles within BISON. The modification is simply a scaling factor of 10^6 as it is related to the atomic jump frequencies at grain boundaries being roughly 10^6 larger than the jump frequencies for lattice atoms [15].

5. Assessment and Sensitivity Analysis

The only experimental data available to validate the U_3Si_2 models in BISON at LWR temperatures are the two rodlets that underwent PIE from the Advanced Test Reactor (ATR) irradiations. These rodlets are identified as R4 from the ATF-13 capsule and R6 from the ATF-15 capsule [4]. The experiments are a typical capsule irradiation test, consisting of a fuel rodlet encapsulated inside a stainless-steel capsule. The nominal dimensions of all capsules used in the ATF-1 experiments are found in [43]. Specific details for the R4 and R6 rodlets can be obtained from the design specifications for the experiments. The R4 and R6 rodlets consisted of 12 enriched (5.4 4wt% U-235) U_3Si_2 pellets stacked on top of a single depleted pellet with two additional depleted pellets placed on top of the active length. The

top two depleted pellets were drilled to accommodate melt wires to monitor the temperature during the experiments. In these experiments, the fuel was placed inside ZIRLO^{TM} [4] cladding before being inserted into the stainless-steel capsule. Details on the fabrication of the fuel pellets used in these experiments are discussed in [44].

The power supplied to the fuel rodlets as a function of time is shown in Figure 9. A flat axial profile was assumed in the BISON simulation given the short length of the rodlet. The rodlets were removed from the ATR at a relatively low burnup (17.1 MWd/kgHM for R4 and 19.6 MWd/kgHM for R6 [4]) to perform PIE. For engineering scale simulation comparisons, only limited data exists. Previous experience from research reactor irradiations of U_3Si_2 suggested that, at some point, the fuel will experience runaway swelling [5]. Therefore, measurements focused on dimensional changes of the fuel and cladding, as well as fission gas release. Measurements of fuel dimensional changes were limited to neutron radiography, which illustrated that the fuel experienced no axial growth (elongation) within the resolution of the measurement technique. Cladding profilometry measurements indicated negligible changes from the as-fabricated dimensions, meaning that no contact between the fuel and cladding was observed [4].

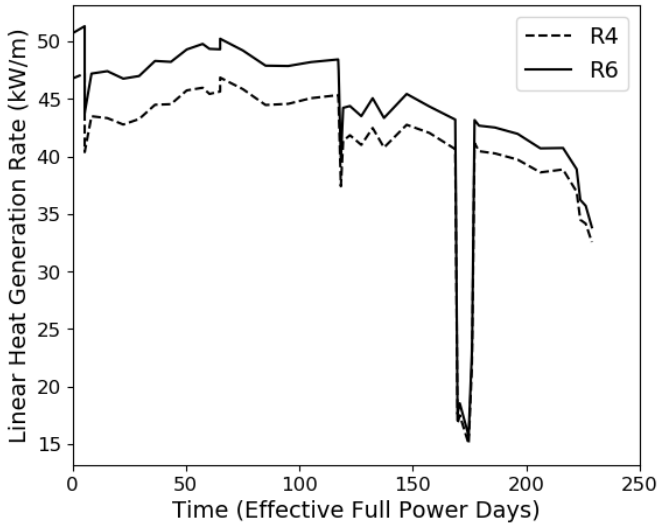

Figure 9: Linear heat generation rate supplied to ATR-13 R4 and ATR-15 R6. Adapted from [4].

A full uncertainty quantification (UQ) and sensitivity study was completed. Table 4 presents the range of applicability, uncertainty, and references for all of the U_3Si_2 models available in BISON as described in Sections 2 and 4. The uncertainties are assumed to represent two standard deviations for the normal distributions. For the uniform and loguniform distributions, any and all values between the upper and lower limits of the range are possible. In the table, T is the temperature and p is the porosity. Further details on the form of the equations and the determination of their uncertainty can be found in [16]. It should be noted that, based upon [45], the grain growth in U_3Si_2 can be ignored. In addition, as mentioned in Section 2.6, densification has been neglected in this study, contrary to previous investigations [16, 17].

To perform the study, the finite element mesh of the drop-in capsule was created using a 2D-RZ axisymmetric smeared pellet mesh assumption. This means that there is an azimuthal plane of symmetry about the rodlet centerline, and the dish and chamfer features of the fuel are not modeled. The insulator pellets – one at the bottom of the stack and two at the top – were included in addition to the ZIRLO^{TM} cladding and stainless-steel capsule. Eleven finite elements were used across the radius of the fuel pellet, with four each through the thickness of the cladding and capsule. Three axial elements per pellet were used, with the cladding and capsule meshes being slightly coarser to ensure improved robustness of the contact algorithm.

The UQ and SA studies were performed by coupling BISON to the Dakota [46] software developed at Sandia National Laboratories. A Latin hypercube sampling (LHS) technique was used to reduce the number of samples required. Two-thousand samples were run for two separate studies, the first using the stoichiometric diffusivities for Xe atoms and Si vacancies, and the second using the Si-rich diffusivities. The results of the study are presented in Table 5 and Figures 10 through 12.

In Table 5 the BISON results are presented as the minimum to maximum value of fuel elongation and fission gas release, assuming two standard deviations about the mean value. The results from a previous study [16] are also included for rodlet R4 only since R6 was not analyzed in the previous work. The results indicate that the new BISON simulations predict a small, non-zero axial change in the fuel stack. While the uncertainty range does not encompass the experimental measurement of zero axial change, it should be noted that the uncertainty of the neutron radiography technique is likely large enough to overlap with the model uncertainty. In addition, recall that a densification model was not included in the BISON analyses, due to the unknown nature of the mechanism in U_3Si_2. If such a model were to be added, it would serve to reduce the total amount of fuel elongation as seen in the results from the previous study [16], which included the standard UO_2 densification model proposed to be used by [17] for U_3Si_2. For fission gas release, it is observed that the experimental values are captured within uncertainty for all cases (both the present and previous studies). The improvements in fission gas modeling utilized in this work results in a small reduction in the upper bounds of the predicted FGR. The uncertainty in predictions for such low release values has been determined to be very large in terms of calculated to measured FGR ratio [47]. The study completed here is said to be an improvement on the previous analysis for three reasons: (1) the study is more comprehensive as it accounts for uncertainty in the Si-rich and stoichiometric diffusivities as well as all of the thermo-mechanical models available in BISON, (2) the uncertainty in some of the fission gas model parameters (e.g., semi-dihedral angle of inter-granular bubbles and saturation coverage of grain boundaries) has been reduced due to the lower length scale improvements described in 4, and (3) this work includes the new mechanistic creep model for U_3Si_2 [13].

Figure 10 presents the evolution of the fuel centerline temperature as a function of time. Both the Rodlets R4 and R6 are

Table 4: Summary of U_3Si_2 models available in BISON, including range of applicability, uncertainty, and the distribution used in the uncertainty quantification and sensitivity analyses of the assessment cases.

Model	Range of Applicability	Uncertainty	References	Distribution
Thermal conductivity	13 K $\leq T \leq$ 1500 K	$\pm$18.2%	[19]	Normal
Specific heat capacity	293 K $\leq T \leq$ 1500 K	$\pm$ 3%	[19]	Normal
Young's modulus	1.5% $\leq p \leq$ 10%	$\pm$ 29.1%	[19]	Normal
Poisson's ratio	1.5% $\leq p \leq$ 10%	$\pm$ 26.8%	[19]	Normal
Thermal expansion	273 K $\leq T \leq$ 1473 K	$(16.0 \pm 3.0) \times 10^{-6}$	[19]	Normal
Solid swelling	All burnups	$\pm$ 20%	[28, 29]	Normal
Xe and vacancy diffusion thermal coefficients	Normal operating conditions	Factor of 7.4		Uniform
Xe and vacancy thermal activation energies	Normal operating conditions	$\pm$ 0.15 eV		Uniform
Xe and vacancy athermal coefficients	Normal operating conditions	Factor of 5		Uniform
Fission gas release and gaseous swelling	Normal operating conditions	[1]Factor of 10^{-3} to 10^4	[15]	Loguniform
	Normal operating conditions	[2]Factor of 0.1 to 10	[15]	Uniform
	Normal operating conditions	[3] $\pm$ 50%	[15]	Uniform
	Normal operating conditions	[4]Factor of 10^{-3} to 10^3	[15]	Loguniform
	Normal operating conditions	[5]Factor of 0.5 to 1	[15]	Uniform
	Normal operating conditions	[6] 0.6 $\pm$ 0.072	[15]	Normal

[1]Applied to the nucleation factor of intra-granular bubbles. [2]Applied to the re-solution rate of intra-granular bubbles. [3]Applied to the U_3Si_2/gas specific surface energy. [4]Applied to the initial number density of inter-granular bubbles. [5]Applied to the semi-dihedral angle of inter-granular bubbles. [6]Applied to the saturation coverage of grain boundaries.

Table 5: BISON comparisons to PIE data for ATF-13 R4 and ATF-15 R6 [4]. The results for R4 from an earlier study [16] is also included for comparison.

	BISON				Experiment	
	R4		R6		R4	R6
	Stoichiometric	Si-Rich	Stoichiometric	Si-Rich		
Fuel elongation (mm)	0.067 to 0.195	0.055 to 0.187	0.091 to 0.267	0.055 to 0.282	0.0	0.0
Fission gas release (/)	0.0 to 0.011	0.0 to 0.004	0.0 to 0.020	0.0 to 0.018	0.0006	0.0006
Fuel elongation (mm) [16]	-0.135 to 0.132	-0.131 to 0.057	N/A	N/A	0.0	0.0
Fission gas release (/) [16]	0.0 to 0.014	0.0 to 0.009	N/A	N/A	0.0006	0.0006

shown with both the results from using the Si-rich and stoichiometric diffusivities. It is observed that as a function of time the temperature continually decreases despite minor variations in power (except for the lower power operation around 175 effective full power days). This decrease in centerline temperature with increase irradiation time is associated with progressive gap closure and consistent with the results of [17], which showed a continual decrease in fuel centerline temperature at a constant power of 20 kW/m until fuel-to-cladding contact occurred around 25 MWd/kgU, after which the temperature remains relatively constant. For Rodlets R4 and R6 the discharge burnups were well below this threshold value (fuel-to-cladding did not occur) and therefore this flattening of the temperature profile is never observed. Moreover, the temperature predictions in this work (see Figure 10) are on average ~200 K higher than those from [17] due to the average linear heat rate being more than twice as large (40-50 kW/m versus 20 kW/m). However, this is encouraging since the predicted temperatures remain below the centerline temperature of the UO_2 rodlet analyzed in [17] (~1400 K) despite the large difference in average linear heat rate.

Figures 11 and 12 illustrate the Spearman correlation coefficients for the stoichiometric and Si-rich fission gas diffusivities respectively. Spearman correlation coefficients were chosen because some of the uncertain inputs have orders of magnitude variation. These coefficients can identify monotonic relationships between inputs and outputs and are always between -1.0 and 1.0. A larger negative value indicates that, as the uncertain input is increased, the corresponding output of interest decreases. Conversely, a larger positive value indicates a positive monotonic relationship between the input and output. A correlation value close to 0.0 indicates no monotonic relationship. A statistically significant relationship between an input and output is assumed to occur when the absolute value of the correlation coefficient is greater than 0.33.

It is observed that the trends of the Spearman correlation coefficients are the same whether or not the diffusivities used for the fission gas atoms and vacancies in the fission gas model are treated as stoichiometric or Si-rich. One sees a moderate effect due to the power (and correspondingly temperature) differences between Rodlets R4 and R6 (e.g., thermal conductivity and the coefficient of thermal expansion). The most significant relation-

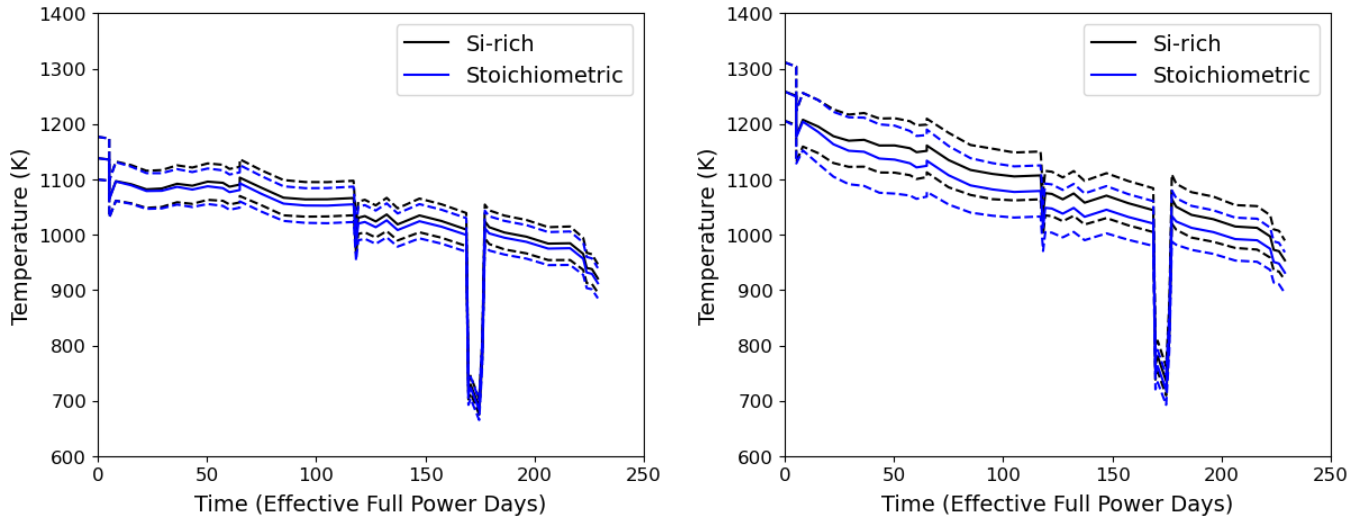

(a) (b)

Figure 10: Predicted centerline temperatures for (a) R4 and (b) R6 using the stoichiometric and Si-rich diffusivities. The solid line corresponds to the mean value and the dashed lines represent $\pm 2\sigma$.

ships with fuel elongation are possessed by the intra-granular nucleation factor, the vacancy diffusion activation energy, the solid swelling factor, the coefficient of thermal expansion, and the thermal conductivity. For fission gas release, the significant input parameters are the intra-granular nucleation factor, the vacancy diffusion activation energy, the inter-granular bubbles dihedral angle, and the intra-granular re-solution rate. Performing additional lower length scale calculations or separate effects experiments for these parameters will help reduce the uncertainty in the inputs and correspondingly improve predictions of the outputs of interest.

6. Conclusions

Experimental data is limited on the behavior of U_3Si_2 under irradiation at LWR operating temperatures. To address this issue, an effort to develop lower length scale informed models of U_3Si_2 fuel behavior for use in the engineering scale fuel performance code BISON was undertaken. The recommended available models in BISON were summarized including the final form of the aforementioned lower length scale informed models. The range of applicability, uncertainty, and distributions assumed for uncertainty quantification and sensitivity analyses was provided. The development and determination of uncertainty of the models presented for thermal conductivity, specific heat capacity, thermal expansion, elasticity, and solid swelling was completed elsewhere [16]. The new features presented include the lower length scale informed creep model and updates to the fission gas behavior model. Details on the development of the lower length scale informed creep model used in this is published separately [13].

In order to develop a fission gas behavior model for U_3Si_2, the diffusivity under irradiation conditions must be well known for a wide range of temperatures. Using literature DFT data [10], we have used cluster dynamics simulations to predict the D_1 and D_2 contributions to Xe diffusivity. Using MD simulations, the athermal contribution due to atomic mixing during ballistic cascades (D_3) has also been predicted. Our LLS-informed correlations for the D_1, D_2, and D_3 contributions to Xe diffusivity have been implemented within the physics-based fission gas release model in BISON. In addition, the inter-granular diffusion coefficients of Si vacancies have been fitted to available literature data and are used to determine the gaseous swelling of the fuel.

Separate effects tests on thermal and mechanical properties of U_3Si_2 were used to develop the empirical correlations used in this work. Therefore, assessment could only be completed to the integral rod tests completed in the ATR. By using separate effects validation for empirical model development and the lower length scale calculations for more complicated fuel behavior, the assessment to the only available integral rod tests could be performed. The results of the uncertainty quantification and sensitivity analyses indicated good agreement with fission gas release measurements and slight overprediction of fuel elongation. This overprediction highlights the necessity of a densification model specific for U_3Si_2 fuel. The most sensitive parameters for fuel elongation calculations were the intra-granular nucleation factor, the vacancy diffusion activation energy, the solid swelling factor, the coefficient of thermal expansion, and the thermal conductivity. The most sensitive parameters for fission gas release calculations included the intra-granular nucleation factor, the vacancy diffusion activation energy, the inter-granular bubbles dihedral angle, and the intra-granular re-solution rate.

7. Acknowledgments

This work was funded by the US Department of Energy under both the Nuclear Energy Advanced Modeling and Simulation (NEAMS) and Consortium for Advanced Simulation of Light Water Reactors (CASL) programs. The submitted manuscript

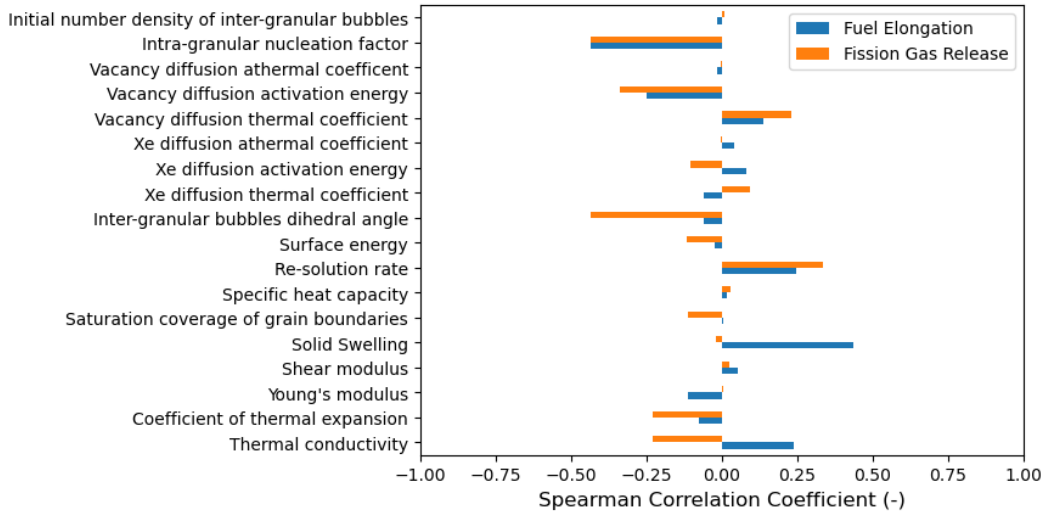

(a)

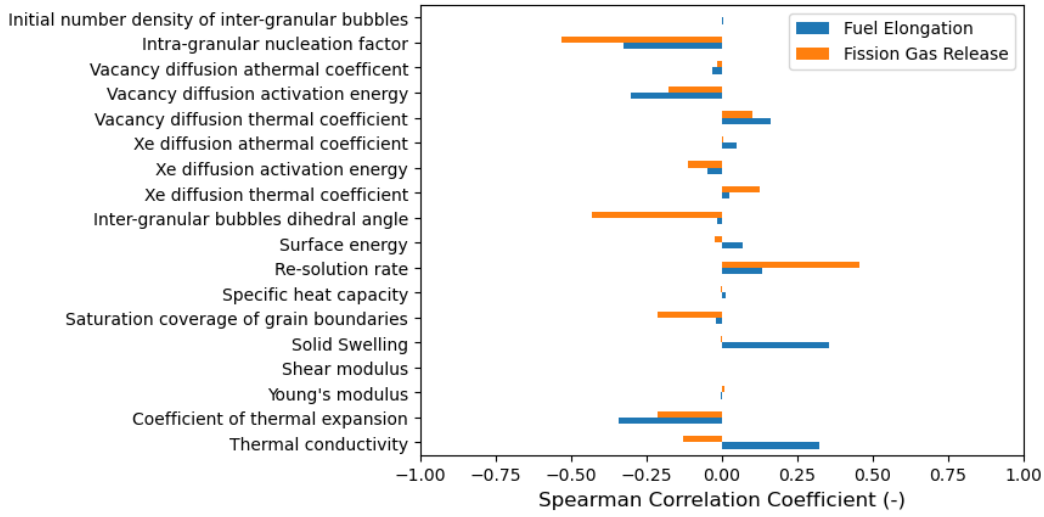

(b)

Figure 11: Spearman correlation coefficients using the stoichiometric diffusivities for (a) Rod R4 and (b) Rod R6.

has been authored by a contractor of the U.S. Government under Contract DE-AC07-05ID14517. Accordingly, the U.S. Government retains a non-exclusive, royalty free license to publish or reproduce the published form of this contribution, or allow others to do so, for U.S. Government purposes.

Los Alamos National Laboratory, an affirmative action/equal opportunity employer, is operated by Triad National Security,LLC, for the National Nuclear Security Administration of the U.S. Department of Energy under Contract No. 89233218CNA000001.

This research made use of the resources of the High Performance Computing Center at Idaho National Laboratory, which is supported by the Office of Nuclear Energy of the U.S. Department of Energy and the Nuclear Science User Facilities under Contract No. DE-AC07-05ID14517.

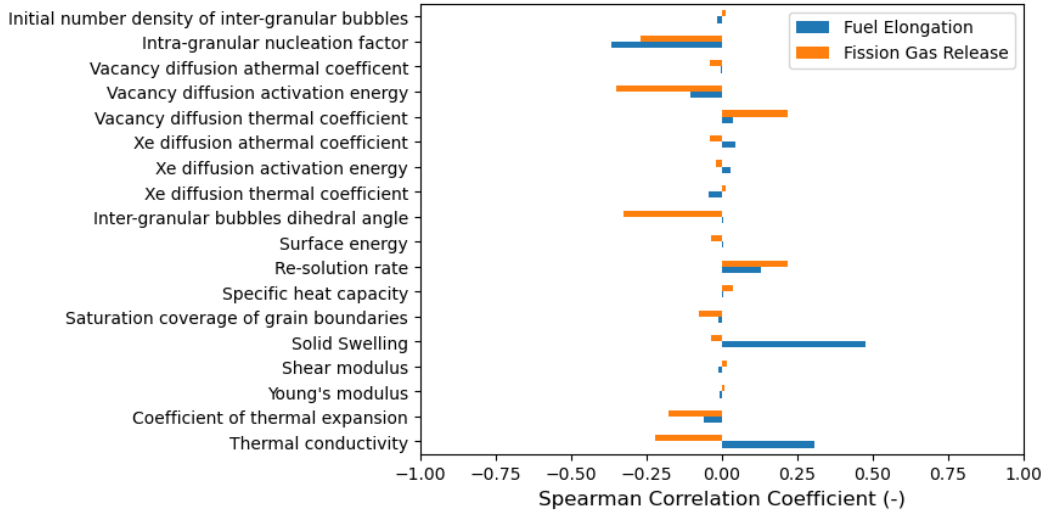

(a)

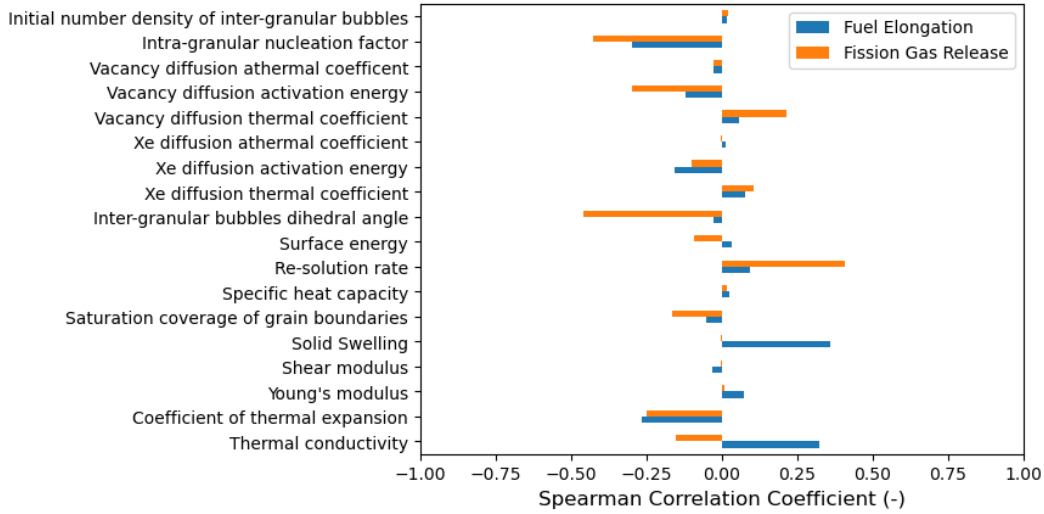

(b)

Figure 12: Spearman correlation coefficients using the Si-rich diffusivities for (a) Rod R4 and (b) Rod R6.

References

[1] H. Shah, J. Romero, P. Xu, R. Oelrich, J. Walters, J. Wright, and W. Gassmann. Westinghouse-Exelon EnCore® Fuel Lead Test Rod (LTR) Program including Coated cladding Development and Advanced Pellets. In *Proceedings of TopFuel 2018*, 2018.

[2] K. Pasamehmetoglu and others. State-of-the-Art Report on Light Water Reactor Accident-Tolerant Fuels. Technical Report 7317, OECD-NEA, 2018.

[3] H. Shimizu. The properties and irradiation behavior of U_3Si_2. Technical Report NAA-SR-10621, Atomics International, 1965.

[4] F. Cappia and J. M. Harp. Postirradiation examination of low burnup U_3Si_2 fuel for light water reactor applications. *Journal of Nuclear Materials*, 518:62–79, 2019. Corrigendum published in Journal of Nuclear Materials 523:538, 2019.

[5] M. R. Finlay, G. L. Hofman, and J. L. Snelgrove. Irradiation behaviour of uranium silicide compounds. *Journal of Nuclear Materials*, 325:118–128, 2004.

[6] R. C. Birtcher, J. W. Richardson, and M. H. Mueller. Amorphization of U_3Si_2 by ion or neutron irradiation. *Journal of Nuclear Materials*, 230(2):158–163, 1996.

[7] Y. Miao, J. Harp, K. Mo, S. Bhattacharya, P. Baldo, and A. M. Yacout. Short communication on "in-situ TEM ion irradiation investigations on U_3Si_2 at LWR temperatures. *Journal of Nuclear Materials*, 484:168–173, 2017.

[8] Y. Miao, J. Harp, K. Mo, S. Zhu, T. Yao, J. Lian, and A. M. Yacout. Bubble morphology in U_3Si_2 implanted by high-energy Xe ions at 300°C. *Journal of Nuclear Materials*, 495:146–153, 2017.

[9] Y. Miao, J. Harp, K. Mo, Y. S. Kim, S. Zhu, and A. M. Yacout. Microstructure investigations of U_3Si_2 implanted by high-energy Xe ions at 600°C. *Journal of Nuclear Materials*, 2017.

[10] D. A. Anderson, X.-Y. Liu, B. Beeler, S. C. Middleburgh, A. Claisse, and C. R. Stanek. Density functional theory calculations of self- and Xe diffusion in U_3Si_2. *Journal of Nuclear Materials*, 515:312–325, 2019.

[11] C. Matthews, R. Perriot, M. W. D. Cooper, C. R. Stanek, and D. A. Andersson. Cluster dynamics simulation of xenon diffusion during irradiation in UO_2. *Journal of Nuclear Materials*, 540:152326, 2020.

[12] M. W. D. Cooper, C. R. Stanek, J. A. Turnbull, B. P. Uberuaga, and D. A. Andersson. Simulation of radiation driven fission gas diffusion in UO_2, ThO_2 and PuO_2. *Journal of Nuclear Materials*, 481:125–133, 2016.

[13] M. W. D. Cooper, K. A. Gamble, L. Capolungo, C. Matthews, B. Beeler, C. R. Stanek, and K. Metzger. Irradiation-enhanced diffusion and diffusion-limited creep in U_3Si_2. *Journal of Nuclear Materials*, In Progress, 2021.

[14] R.L. Williamson, K.A. Gamble, D.M. Perez, S.R. Novascone, G. Pastore, R.J. Gardner, J.D. Hales, W. Liu, and A. Mai. Validating the BISON fuel performance code to integral LWR experiments. *Nuclear Engineering and Design*, 301:232 – 244, 2016.

[15] T. Barani, G. Pastore, D. Pizzocri, D.A. Andersson, C. Matthews, A. Alfonsi, K.A. Gamble, P. Van Uffelen, L. Luzzi, and J.D. Hales. Multiscale modeling of fission gas behavior in U_3Si_2 under LWR conditions. *Journal of Nuclear Materials*, 522:97–110, 2019.

[16] K. A. Gamble, G. Pastore, M. W. D. Cooper, and D. Andersson. ATF material model development and validation for priority fuel concepts. Technical Report CASL-U-2019-1870-000 Rev.0, Idaho National Laboratory, 2019.

[17] K. E. Metzger, T. W. Knight, and R. L. Williamson. Model of U_3Si_2 fuel system using BISON fuel code. In *Proceedings of the International Congress on Advances in Nuclear Power Plants - ICAPP 2014*, Charlotte, NC, April 6–9 2014.

[18] W. Li and K. Shirvan. U_3Si_2-SiC fuel performance analysis in BISON during normal operation. *Annals of Nuclear Energy*, 132:34–45, 2019.

[19] J. T. White. Update to the U_3Si_2 property handbook. Technical Report LA-UR-18-28719, Los Alamos National Laboratory, 2018.

[20] J. T. White, A. T. Nelson, J. T. Dunwoody, D. J. Safarik, and K. J. McClellan. Corrigendum to Thermophysical Properties of U_3Si_2 to 1773 K. *Journal of Nuclear Materials*, 484:386–387, 2017.

[21] A. Mohamad, Y. Ohishi, H. Muta, K. Kurosaki, and S. Yamanaka. Thermal and mechanical properties of polycrystalline U_3Si_2 synthesized by spark plasma sintering. *Journal of Nuclear Science and Technology*, 55(10):1141–1150, 2018.

[22] D. Antonio, K. Shrestha, J. Harp, C. Adkins, Y. Zhang, J. Carmack, and K. Gofryk. Thermal and transport properties of U_3Si_2. *Journal of Nuclear Materials*, 508:154–158, 2018.

[23] J. T. White, A. T. Nelson, J. T. Dunwoody, D. D. Byler, D. J. Safarik, and K. J. McClellan. Thermophysical properties of U_3Si_2 to 1773K. *Journal of Nuclear Materials*, 464:275–280, 2015.

[24] E. G. Obbard and K. D. Johnson and P. A. Burr and D. A. Lopes and D. J. Gregg and K.-D. Liss and G. Griffiths and N. Scales and S. C. Middleburgh. Anisotropy in the thermal expansion of uranium silicide measured by neutron diffraction. *Journal of Nuclear Materials*, 508:516–520, 2018.

[25] R. A. Freeman, T. Martin, E. Roberts, and T. W. Knight. Analysis of thermal creep for uranium silicide fuel using Bison. In *Proceedings of the 2018 International Congress on Advances in Nuclear Power Plants (ICAPP 18)*, Charlotte, NC, 2018.

[26] K. E. Metzger. *Analysis of Pellet Cladding Interaction and Creep of U_3Si_2 Fuel for use in Light Water Reactors*. PhD thesis, University of South Carolina, 2016.

[27] E. A. C. Mercado. High temperature compression creep of U_3Si_2. Master's thesis, University of South Carolina, 2018.

[28] G. L. Hofman and W. S. Ryu. Detailed Analysis of Uranium Silicide Dispersion Fuel Swelling. Technical Report CONF-8909141–10, Argonne National Laboratory, 1989.

[29] T. Ikonen and V. Tulkki. The importance of input interactions in the uncertainty and sensitivity analysis of nuclear fuel behavior. *Nuclear Engineering and Design*, 275:229–241, 2014.

[30] I. Greenquist and M. Tonks and Y. Zhang. Analysis of the impact of fuel microstructure on irradiation-enhanced densification using grand potential simulations. *Annals of Nuclear Energy*, 151:107858, 2021.

[31] C. Matthews, R. Perriot, M. W. D. Cooper, C. R. Stanek, and D. A. Andersson. Cluster dynamics simulation of uranium self-diffusion during irradiation in UO_2. *Journal of Nuclear Materials*, 527:151787, 2019.

[32] S. Plimpton. Fast Parallel Algorithms for Short – Range Molecular Dynamics. *Journal of Computational Physics*, 117(June 1994):1–19, 1995.

[33] B. Beeler, M. Baskes, D. Andersson, M. W. D. Cooper, and Y. Zhang. A modified Embedded-Atom Method interatomic potential for uranium-silicide. *Journal of Nuclear Materials*, 495:267–276, 2017.

[34] B. Beeler, D. A. Andersson, M. W. D. Cooper, and Y. Zhang. A molecular dynamics study of the behavior of Xe in U3Si2. *Journal of Nuclear Materials*, 523:413–420, 2019.

[35] B. Beeler, M.W.D. Cooper, Z.-G. Mei, D. Schwen, and Y. Zhang. Radiation driven diffusion in γU-Mo. *Journal of Nuclear Materials*, 543:152568, 2021.

[36] C. Matthews, D. Schwen, and A. C. Klein. Radiation re-solution of fission gas in non-oxide nuclear fuel. *Journal of Nuclear Materials*, 457:273–278, 2015.

[37] S. C. Middleburgh, R. W. Grimes, E. J. Lahoda, C. R. Stanek, and D. A. Andersson. Non-stoichiometry in U_3Si_2. *Journal of Nuclear Materials*, 482:300–305, 2016.

[38] J. A. Turnbull and C. A. Friskney and J. R. Findlay and F. A. Johnson and A. J. Walter. The diffusion coefficients of gaseous and volatile species during the irradiation of uranium dioxide. *Journal of Nuclear Materials*, 107:168–184, 1982.

[39] J. A. Turnbull and R.T. White and C. Wise. The diffusion coefficient for fission gas atoms in uranium dioxide. In *Proceedings of the Water Reactor Fuel Element Computer Modeling in Steady State, transient and accident conditions*, pages 174–181, 1988.

[40] G. Pastore, L. Luzzi, V. Di Marcello, and P. Van Uffelen. Physics-based modelling of fission gas swelling and release in UO_2 applied to integral fuel rod analysis. *Nuclear Engineering and Design*, 256:75–86, 2013.

[41] B. Beeler, M. Baskes, D. Andersson, M.W.D. Cooper, and Y. Zhang. Molecular dynamics investigation of grain boundaries and surfaces in U_3Si_2. *Journal of Nuclear Materials*, 514:290–298, 2019.

[42] L. K. Aagesen, D. Andersson, B. W. Beeler, M. W. D. Cooper, K. A. Gamble, Y. Miao, G. Pastore, and M. R. Tonks. Phase-field simulations of intergranular fission gas bubble behavior in U_3Si_2 nuclear fuel. *Journal of Nuclear Materials*, 541:152415, 2020.

[43] K. E. Barrett, K. D. Ellis, C. R. Glass, G. A. Roth, M. P. Teague, and J. Johns. Critical processes and parameters in the development of accident tolerant fuels drop-in capsule irradiation tests. *Nuclear Engineering and Design*, 294:38–51, 2015.

[44] J. M. Harp, P. A. Lessing, and R. E. Hoggan. Uranium silicide pellet

fabrication by powder metallurgy for accident tolerant fuel evaluation and irradiation. *Journal of Nuclear Materials*, 466:728–738, 2015.

[45] A. Cheniour, M. R. Tonks, B. Gong, T. Yao, L. He, J. M. Harp, B. Beeler, Y. Zhang, and J. Lian. Development of a grain growth model for u_3si_2 using experimental data, phase field simulation and molecular dynamics. *Journal of Nuclear Materials*, 532:152069, 2020.

[46] B. M. Adams, L. E. Bauman, W. J. Bohnhoff, K. R. Dalbey, M. S. Ebeida, J. P. Eddy, M. S. Eldred, P. D. Hough, K. T. Hu, J. D. Jakeman, J. A. Stephens, L. P. Swiler, D. M. Vigil, and T. M. Wildey. Dakota, a multilevel parallel object-oriented framework for design optimization, parameter estimation, uncertainty quantification, and sensitivity analysis: Version 6.11 user's manual. Technical Report SAND2014-4633, Sandia National Laboratories, 2019.

[47] G. Pastore, L. P. Swiler, J. D. Hales, S. R. Novascone, D. M. Perez, B. W. Spencer, L. Luzzi, P. Van Uffelen, and R. L. Williamson. Uncertainty and sensitivity analysis of fission gas behavior in engineering-scale fuel modeling. *Journal of Nuclear Materials*, 456:398–408, 2015.